Annealing effects on the photoluminescence of terbium doped zinc oxide films

Ahmed Ziani, Christian Davesnne, Christophe Labbé, Julien Cardin, Philippe Marie, Xavier Portier, Cedric Frilay, Sophie Boudin

HAL Id: hal-01138059

https://hal.science/hal-01138059

Submitted on 13 Apr 2017

Annealing effects on the photoluminescence of terbium doped zinc oxide films

A. Ziani [a],[*], C. Davesnne [a], C. Labbé [a], J. Cardin [a], P. Marie [a], C. Frilay [a], S. Boudin [b], X. Portier [a]

[a] *CIMAP, CEA/UMR CNRS 6252/ENSICAEN/Université de Caen Basse Normandie 6, Boulevard Maréchal Juin, 14050 Caen, France*
[b] *CRISMAT, UMR CNRS 6508/ENSICAEN/Université de Caen Basse Normandie 6, Boulevard Maréchal Juin, 14050 Caen, France*

ABSTRACT

Terbium doped zinc oxide (Tb:ZnO) films were deposited by radio frequency magnetron sputtering on (100) single-crystalline silicon substrates at low temperature ($T_S = 100$ °C). In this work, structural changes, optical properties and the associated photoluminescence (PL) responses are analyzed upon the annealing treatments. Post-annealing treatments from annealing temperature $T_a = 400$ °C up to 1000 °C by steps of 100 °C were performed. Chemical analyses by energy dispersive X-ray spectrometry measurements showed a constant dopant concentration of 3 at.%. Up to 600 °C, the band gaps (E_g) decreased with T_a from 3.44 down to 3.37 eV. Above 600 °C, the band gap raised from 3.37 up to 3.42 eV (for 900 °C). Depending on T_a, a bi-axial stress was found varying from a compressive value of -0.21 GPa (400 °C) down to a tensile value of 0.05 GPa (1000 °C). PL mechanisms of the Tb:ZnO film are then discussed.

1. Introduction

Among the various materials used in the microelectronic industry, zinc oxide (ZnO) is a promising material due to its high electron mobility, good thermal conductivity, wide and direct band gap and large exciton binding energy. This material is already used in many applications, including transparent thin-film transistors, photodetectors, light-emitting diodes (LED) and laser diodes. Furthermore, it is a cheap and environmentally safe material. In the field of optoelectronic industry, ZnO thin films are the object of numerous studies [1,2]. ZnO, electrically or optically excited, emits in the UV spectral range due to its band gap (3.36 eV) as well as in the blue/green spectral region originating from intrinsic defects in the matrix. Doped ZnO with rare earth elements (RE:ZnO) can also emit in the visible spectral range. For instance, a red emission is observed with Europium (Eu^{3+}) doping [3,4] and a green one is achieved by Terbium (Tb^{3+}) doping [3]. Based on the contribution of intrinsic defects and RE emissions created in the ZnO matrix, white light emission can be obtained. The ultimate goal is to demonstrate the possibility of a monolithic LED based on RE:ZnO materials.

ZnO films are materials used for various applications [5], but there are only a few studies focused on Tb doping of ZnO [6,7]. Most of the time, ZnO doping is performed with group III elements such as Bore

(B), Gallium (Ga), Indium (In) or Aluminum (Al) [8], leading to an improvement of its electrical conductivity. To a lesser extent, rare earth doping is also found to improve the electrical conductivity of ZnO. Fang et al. [6], who worked on the growth of ZnO thin films by reactive radiofrequency magnetron sputtering (RMS) with a Tb concentration of 4.1 at.%, found that the electrical resistivity decreases from $9.4 \cdot 10^{-3}$ Ω·cm for undoped films down to $9.3 \cdot 10^{-4}$ Ω·cm for Tb doped films and keeping a good optical transparency. Beyond this doping level and similarly to the case of group III dopants, transport properties of ZnO are deteriorated. As far as optical properties are concerned, the control of different rare earth doping concentrations provides an original way to obtain a monitored spectral distribution of the total luminescence. Other papers deal with the effect of various annealing treatments on the improvement of photoluminescence (PL) and structural properties of the films. Teng et al. [7] showed an increasing PL intensity of ZnO defects (green emission) in Tb:ZnO thin films grown by RMS as a function of annealing temperature (T_a). Otherwise, other works dealing with Tb doping in ZnO powders [9], ZnO thin films synthesized by dip coating [10], electrodeposition [11] or spray pyrolysis [12] are also reported in literature. Similar studies of Tb:ZnO films doped by Tb implantation are also found in previous works [13]. All these works show an improvement of the PL emission intensity related to the optical transitions of Tb^{3+} ions (green emission). In our study, we focus on Tb:ZnO films grown by RMS method and submitted to various annealing treatments. In the following, we emphasize on the resulting structural, optical and PL properties of Tb:ZnO films, and the PL excitation/emission mechanisms are discussed.

2. Experimental details

Tb:ZnO films were grown by RMS using a pure ZnO target. Doping was obtained by placing ten terbium oxide (Tb_4O_7) calibrated pellets on the surface of the ZnO target. This number of pellets corresponded to a given surface ratio of the target and thus to a given concentration of the dopant in the film. Films were grown on (100) silicon (Si) substrates whose temperature was fixed at 100 °C. The total pressure (P_T) and the RF power to target (P_{RF}) were kept equal to 1.5 Pa and 1.91 $W \cdot cm^{-2}$, respectively. Using these parameters, the growth rate was found to be about 9 $nm \cdot min^{-1}$. All post-annealing treatments were carried out during 1 h under continuous nitrogen (N_2) flow at temperatures (T_a) ranging from 400 °C up to 1000 °C and varied by step of 100 °C.

Surface morphology and chemical analysis observation was performed using a Jeol JSM 6400 scanning electron microscopy (SEM) with classical tungsten filament and a voltage of 12 kV. Coupled Oxford Inca Energy coupled Energy Dispersive X ray Spectrometry (EDXS) was used to determine the dopant concentration. X-ray diffraction (XRD) diagrams were recorded using the Bragg–Brentano $\theta - 2\theta$ configuration, on a Philips Xpert NPD Pro diffractometer (Cu K α_1 radiation), with a 0.005° angular step size and with a counting time of 4 s per step. Transmission electron microscopy (TEM) observations were performed using a 2010 FEG JEOL microscope operated at 200 kV.

Thickness and refractive index ($n + ik$) of the films were determined from spectroscopic ellipsometry technique. Measurements were collected by scanning in the 1.5–4.5 eV range by using a Jobin-Yvon Ellipsometer (UVISEL). The energy band gap (E_g) was calculated using the Tauc formalism [14]. We plotted absorption α^2 as a function of energy considering the linear region of the plot down to zero loss value and found the E_g value with an error of about 0.01 eV.

The photoluminescence (PL) emission and PL excitation (PLE) measurements were collected by a Jobin-Yvon Fluorolog Spectrofluorometer with a 450 W Xenon lamp as source of excitation.

3. Results and discussion

In this paper, we discuss the annealing temperature effect on the structural and PL properties of Tb:ZnO films. This requires structural and optical characterizations for various films submitted to various annealing treatments. The corresponding PL responses are analyzed and compared to those of an as grown Tb:ZnO film grown in the same sputtering kit. For this purpose, we have grown 1.1 μm thick films, namely: Tb:ZnO-1 corresponds to the as-grown film and Tb:ZnO-(x) with x ranging from 2 to 8 correspond to films annealed at temperatures ranging from 400 °C up to 1000 °C by steps of 100 °C. EDXS measurements (not shown) indicate that the Tb atomic percentage in all ZnO doped films is found almost constant at about 3 at.%.

Fig. 1 shows a series of XRD diagrams for the as-grown and annealed films. We observe a preferred growth orientation of the Tb:ZnO films following the c-axis (00L) denoting a texture of the films. This feature increases with T_a. Furthermore, one can notice a shift of the (002) peak position from 34.11° to 34.53° with T_a. We remind that the expected bulk ZnO (002) position is 34.42°. Below T_a = 800 °C, we see a peak broadening of the full width half maximum (FWHM) varying from 0.26° to 0.46°. For higher T_a values, FWHM decreases down to 0.22° and new peaks related to a new phase are observed in the [28°–32°] range. This new phase could be attributed to a $Zn_xSi_{1-x}O$ phase originating from an Si diffusion across the film/substrate interface.

Fig. 2a and c shows bright field TEM images of the doped films annealed at 600 °C and 900 °C, respectively. Both images reveal a perpendicular columnar growth of the films. The selected area electron diffraction (SAED) patterns shown in Fig. 2b and d confirm a strong (00L) texture. Upon annealing treatment at 900 °C (Fig. 2c), a thin layer of about 50 nm thick is formed at the film/substrate interface. Interpreting the XRD data, this layer may correspond to the $Zn_xSi_{1-x}O_3$ phase. The
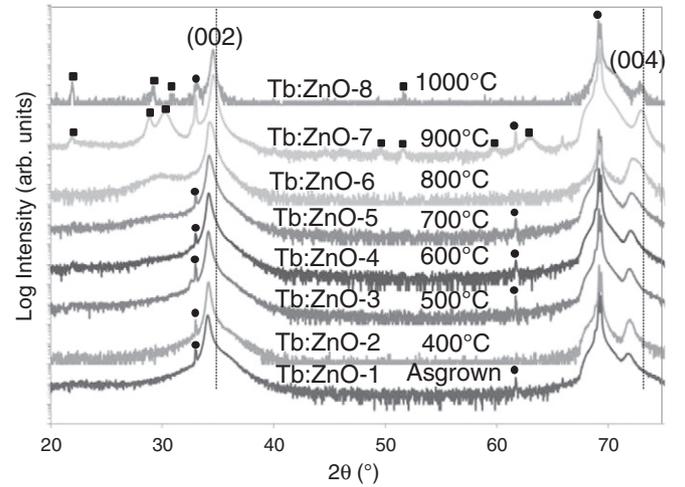

Fig. 1. X-ray diffraction diagrams of as grown Tb:ZnO-1 and annealed thin films from 400 to 1000 °C (Tb:ZnO-2 to Tb:ZnO-8). The peaks labeled as (●) refer to the Si substrate and the peaks labeled as (■) refer to the $Zn_xSi_{1-x}O_3$ phase.

corresponding SAED pattern confirms this new phase by the appearance of two new spots (rings in Fig. 2d). To estimate the grain size, called D, which can be compared to the mean column diameter in ZnO matrix seen in Fig. 2a and c, we used the Scherrer's formula:

$$D = \frac{0.9\,\lambda}{\beta \cdot \cos\theta}$$

with β, the peak width at half height expressed in radians and θ, the diffraction peak position observed.

ZnO has an hexagonal structure and its d_{hkl} spacing is expressed as follows:

$$d_{hkl} = \frac{\lambda}{\sin\theta} = \frac{a}{\sqrt{\frac{4}{3}\left(h^2 + k^2 + hk\right) + l^2 \frac{a^2}{c^2}}}$$

In the case of (002) orientation, the relationship becomes $c = 2d_{hkl} = 2\frac{\lambda}{\sin\theta}$.

When T_a changes, a shift of the (002) peak is observed. As a result, the c values are deduced and a comparison to the theoretical one (c_0 = 5.206 Å in the JCPDS sheet No. 5-664) provides information on the state of stress for the deposited layers. Indeed, taking c_0 as a reference for unconstrained ZnO films, and c for constrained ones, we can calculate strain in the films from the equation:

$$\varepsilon = \frac{c - c_0}{c_0} * 100\,(\%).$$

Then, we deduce the bi-axial stress in the films from the equation that takes into account the elastic constants of ZnO [15]:

$$\sigma = -232.8 \cdot 10^{-9} * \varepsilon\,(Pa).$$

Smooth surfaces are obtained for all the films. By contrast, the film annealed at the highest T_a values (Tb:ZnO-8) is dramatically affected. An important roughness is observed at its surface. Furthermore, the film/substrate interface is not stable mechanically. It's comparable to a sintered powder deposited on Si substrate.

Fig. 3 depicts grain size as well as bi-axial stress versus T_a. The major effect is a decrease of grain size from 32 nm down to 19.5 nm for T_a varying from room temperature up to 800 °C. Above 800 °C, we notice an important increase of grain size. A stress relaxation from −0.18 GPa
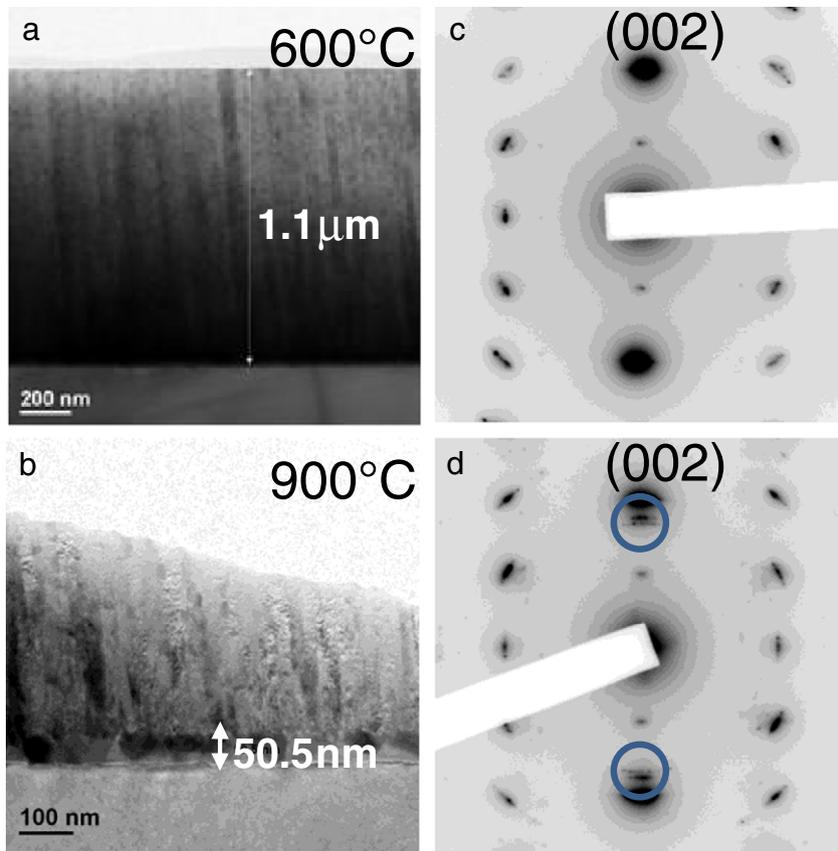
Fig. 2. TEM images and selected area electron diffraction patterns (SAED) of Tb:ZnO films annealed at 600 °C (a, c) and 900 °C (b, d). A thin layer of about 50 nm thick is observed between the Si substrate and the film upon the 900 °C annealing treatment.

down to 0.05 GPa is also observed in the films. These effects are well known and reported in many studies on annealing effects of such films [16,17]. A transition is observed from a compressive to a tensile stress for temperatures higher than 800 °C. This transition could be explained by the appearance of the new phase at the film/substrate interface, which changes the strain configuration at the interface. The characteristics of the films are given in Table 1.

Regarding the optical characterizations, we see that the most visible effect of the annealing treatments is a gradual increase of the refractive index n for T_a values up to 600 °C followed by a collapse at 900 °C (Fig. 4a). Below 600 °C, we observe a rise from 2.42 up to 2.53 (for an energy value of 3 eV). Usually, an increase of n values indicates a higher material density [18], a higher degree of crystallization or a better distribution of the dopants in the matrix as observed in our case. The band
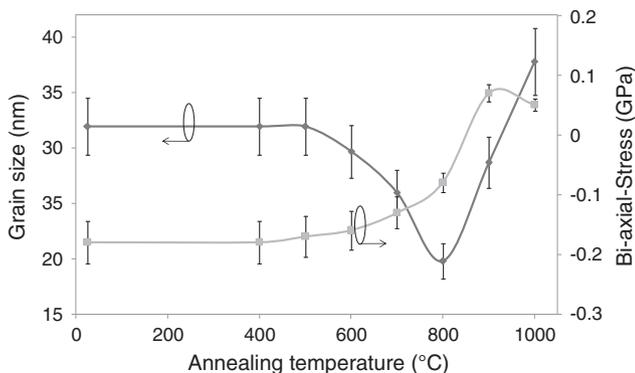
gap follows an opposite trend: it decreases from 3.45 (room temperature) down to 3.37 eV for 600 °C and it rises up to 3.42 eV for 900 °C (Fig. 4b). In the case of $Zn_{1-x}Mg_xO$ nanocrystals [19], it has been shown that higher Mg concentration may result in a rising grain size from 10 to 12 nm and in a decrease of the c ZnO lattice parameter resulting in a band gap increase. Li-Bin et al. [20] found that, for a compressive stress following the c axis, the conduction band moves to higher energy levels leading to higher band gap in $Zn_{0.75}Mg_{0.25}O$. Li et al. [21] also showed a linear dependency of ZnO band gap energy with respect to compressive bi-axial stress. In those studies, the tensile bi-axial stress of ZnO thin films deposited on quartz and annealed from 240 to 800 °C was measured. They found a concomitant increase of bi-axial stress from 1.45 to 2.01 GPa and of band gap energy with annealing temperature. In our case, above 600 °C, we obtain an opposite trend of the evolutions of refractive index and band gap with T_a. This may correspond to the beginning of a coarsening behavior at 800 °C dominated by a diffusion mechanism of V_O and Zn_i in the film leading to the formation of a new phase at the interface [22].

Fig. 5a and b displays PL and PLE spectra, respectively for the various T_a values. As shown in Fig. 5a, up to 600 °C, we observe an increase of the PL emission of $^5D_4 \rightarrow {}^7F_i$ (i = 6, 5, 4, 3) transitions and especially the $^5D_4 \rightarrow {}^7F_5$ (545 nm) one. This maximum intensity observed for 600 °C is coherent with the lowest band gap value of the matrix (maximum absorption) and also with the highest n value (consistent with an homogeneous distribution of the Tb ions in the matrix). Beyond 600 °C, the intensities of these transitions diminish drastically until complete disappearance for T_a = 800 °C. Up to 800 °C, annealing of Tb:ZnO films have led to a better crystallinity of the films (higher degree of texturing). It allowed a biaxial stress relaxation and then a better absorption of ZnO matrix. A better carrier distribution permits a better Tb optical activation. For excitation energies above the band gap of Tb:


Fig. 3. Grain size and bi-axial stress for different annealing temperatures.

Table 1
Characteristics of the annealed Tb:ZnO thin films (T_a = 400 to 1000 °C).

| Sample	Annealing temperature (°C)	FWHM (°)	2θ (°)	Grain size (nm)	c (Å)	Strain (%)	Bi-axial stress (GPa)	PL intensity at 545 nm (Nb of counts)	PL intensity at 385 nm (Nb of counts)	Band gap (eV)	Refractive index (at 3 eV)
Tb:ZnO-1	25	0.26	34.11	31.96 ± 2.48	5.253	−0.91	(−) 0.18 ± 0.02	480	0	3.44 ± 0.01	2.42 ± 0.05
Tb:ZnO-2	400	0.26	34.12	31.96 ± 2.47	5.251	−0.88	(−) 0.18 ± 0.02	1640	0	3.39 ± 0.01	2.43 ± 0.05
Tb:ZnO-3	500	0.26	34.13	31.96 ± 2.47	5.25	−0.85	(−) 0.17 ± 0.02	2830	0	3.38 ± 0.01	2.45 ± 0.05
Tb:ZnO-4	600	0.28	34.15	29.68 ± 2.14	5.247	−0.79	(−) 0.16 ± 0.02	4360	0	3.37 ± 0.01	2.53 ± 0.05
Tb:ZnO-5	700	0.32	34.19	25.97 ± 1.64	5.241	−0.68	(−) 0.13 ± 0.02	1830	0	3.39 ± 0.01	2.39 ± 0.05
Tb:ZnO-6	800	0.42	34.27	19.79 ± 0.95	5.229	−0.45	(−) 0.08 ± 0.02	0	1060	3.41 ± 0.01	2.35 ± 0.05
Tb:ZnO-7	900	0.29	34.58	28.69 ± 1.99	5.184	0.42	0.07 ± 0.02	0	10,800	3.42 ± 0.01	2.25 ± 0.05
Tb:ZnO-8	1000	0.22	34.53	37.82 ± 3.46	5.191	0.28	0.05 ± 0.02	0	138,000	/	/

ZnO, we see a Tb optical activation in the matrix. We showed an optimal Tb activation in ZnO matrix at 600 °C. For temperatures higher than 800 °C (800–1000 °C), the emergence of a PL band at 387 nm is visible and becomes more intense when T_a is raised. This PL peak is clearly attributed to the conduction to valence band transition in ZnO matrix [7]. The Tb PL extinction is progressively decreasing from 600 °C up to 800 °C, temperature from which the signal has completely disappeared. This is most probably due to a "quenching" effect which presumably results from the segregation of Tb ions upon annealing treatment at high temperatures. In the literature, some works on undoped ZnO films showed a degradation of the PL beyond 800 °C and demonstrated also the appearance of a large band around 500 nm due to an increase of defect density. This PL defect states related do not appear in our spectra. For temperatures higher than 800 °C, the diffusion of chemical species in the matrix attenuates the texturing effect and subsequently disturbs

Fig. 4. (a) Refractive indices of Tb:ZnO films at E = 3 eV annealed at different temperatures from 400 to 1000 °C, (b) band gap versus annealing temperature.

the carriers' distribution. To investigate these phenomena in more details with temperature, we performed PLE spectra with respect to T_a for Tb:ZnO (as-grown, 600 °C and 900 °C) and undoped ZnO (annealed at 600 °C) films. Regarding the PLE measurements (Fig. 5b) with a detection wavelength at 490 nm ($^5D_4 \rightarrow {}^7F_6$) for Tb^{3+}, we observe for undoped ZnO annealed at 600 °C as well as for as grown and annealed at 900 °C Tb:ZnO films two broad peaks centered at 282 and 380 nm. These two levels correspond to 4f → 5d transitions of Tb^{3+} ions and to ZnO host matrix, respectively [23–25]. At 900 °C, we see a PLE signal almost similar to that observed for undoped ZnO films, meaning that Tb ions are not active. For the as grown Tb:ZnO films, the two levels are weak and demonstrate that an annealing treatment is necessary to activate the dopants. For T_a = 600 °C, we note an intense response of the 4f → 5d transition indicating an effective Tb activation due to the defect passivation. However, the peak at 380 nm has disappeared suggesting that the ZnO matrix is not contributing to the Tb excitation. Regarding the Tb excitation/emission mechanisms below 600 °C, we refer to two ways of Tb emissions. Several models of Tb emission/excitation mechanisms in ZnO are proposed in the literature depending on the scale of ZnO material (particle size, film structures) [9–11,26–28]. In these studies, the emission process takes place via an energy transfer occurring from the host matrix to the Tb^{3+} ions, from the conduction band directly or through matrix defects. This process is more relevant for Tb ions well incorporated in the crystalline structure of the ZnO host matrix. However, these mechanisms in Tb:ZnO films are still a matter of debate. Another process is generated directly through Tb^{3+} ions emitting via its energy levels. This is the case for matrices with a large band gap requiring high excitation energy [29,30].

To investigate the energy transfer mechanism in our doped annealed films, we report, in Fig. 6a, PL spectra of the Tb:ZnO film annealed at 600 °C at different excitation wavelengths (415, 330, 350 and 282 nm). (i) The 415 nm wavelength is nonresonant with the RE dopant. We detect a broad PL band in the 390 nm–650 nm spectral range. This emission is usually attributed to zinc and/or oxygen vacancies and interstices in ZnO matrix [31]. In order to know whether these emissions [390 nm–650 nm] are originating from ZnO host defects or the $^5D_3 \rightarrow {}^7F_i$ Tb transitions [30,32,33], we compared a Tb:ZnO film annealed at 600 °C to a very thick (4 μm) undoped ZnO film (Fig. 6b). For an excitation at 330 nm, we observed a superposition of the PL contribution from the defects of undoped ZnO and that of Tb:ZnO film. This result proves that the 395, 415 438, 470, and 508 nm PL peaks come from the ZnO defects [31]. Furthermore, the PL emission peaks are not interference effect and we do not observe any transfer from the defects towards the dopants. (ii) At 385 nm in Fig. 6a, below the conduction band of ZnO, we still detect the defect signature but more intensely. (iii) At 350 nm, above the ZnO band gap but non-resonant with the Tb dopant, we detect once again the defect signature but we also see the presence of $^5D_4 \rightarrow {}^7F_i$ (i = 6, 5, 4, 3) peaks related to Tb energy levels. (iv) When the sample is excited at 282 nm, Tb ions and defects in ZnO matrix are both emitting due to a better distribution of the free carriers in ZnO host matrix. Indeed, intense PL signals are observed due to a direct Tb excitation.
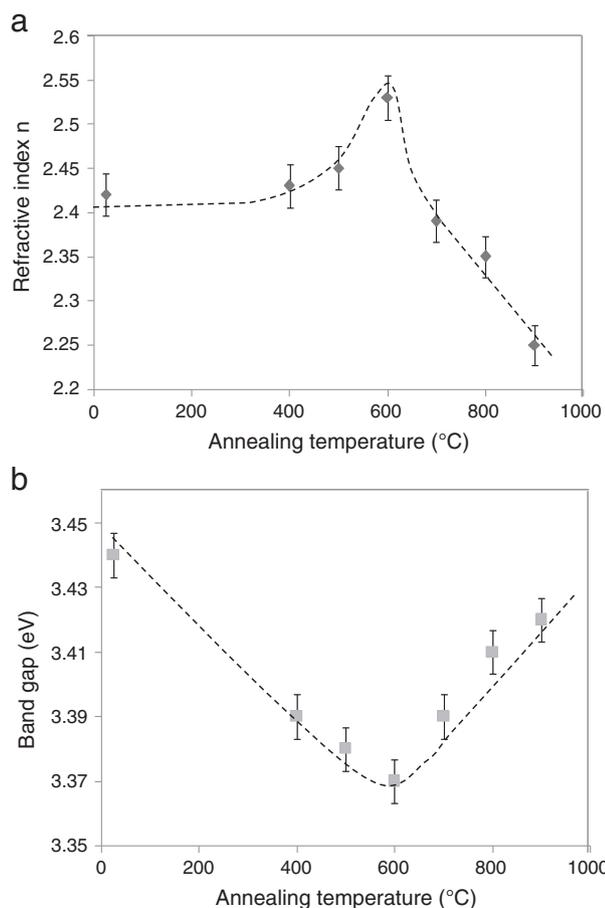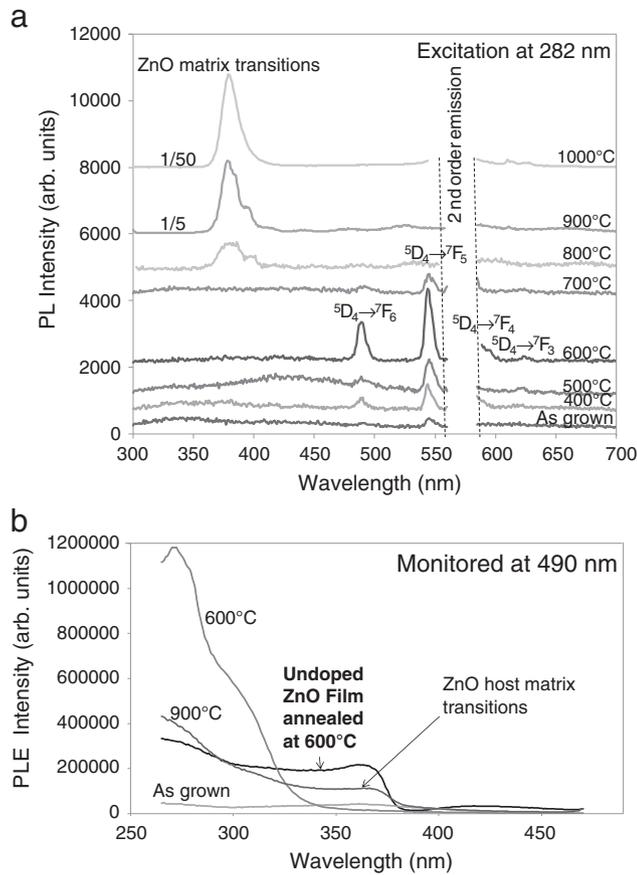
Fig. 5. (a) PL spectra of the annealed Tb:ZnO samples with excitation wavelength at 282 nm and (b) PLE spectra with detection wavelength at 490 nm of Tb ZnO films as grown, annealed at 600 °C, annealed at 900 °C and undoped ZnO film.

Fig. 6. (a) PL spectra of Tb:ZnO annealed at 600 °C with different excitation between 282 nm and 415 nm and (b) comparison between Tb:ZnO and a undoped ZnO films grown with similar conditions with excitation at 330 nm.
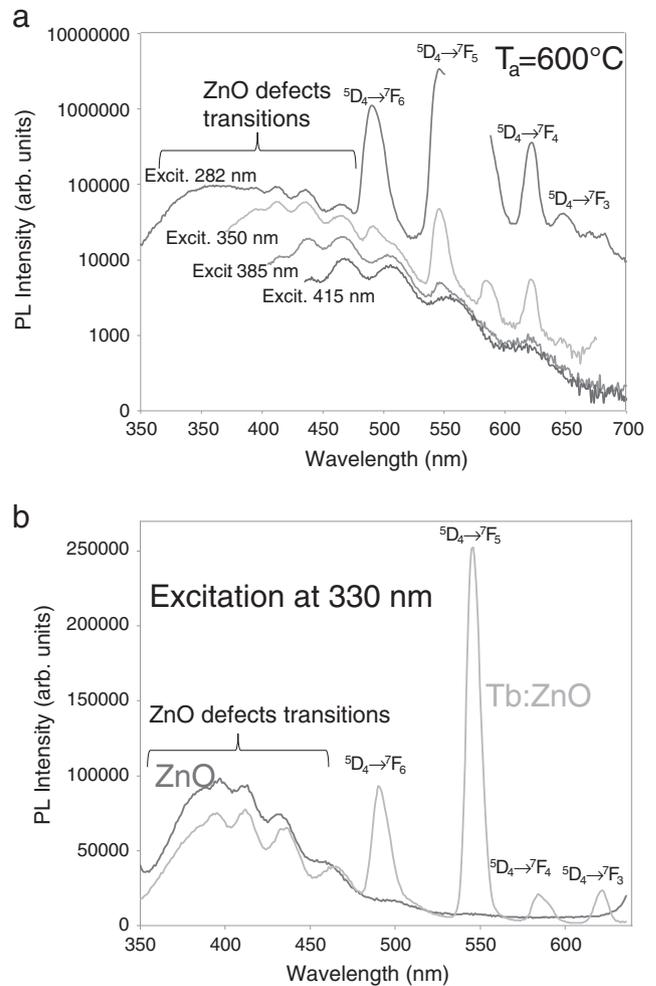
4. Conclusion

In this work, we analyzed the annealing treatment effect on the photoluminescence properties of Tb:ZnO films with a doping rate of 3 at.%. Thermal annealing up to 600 °C resulted in an optimum emission of the Tb D_{levels} such as the radiative transitions $^5D_4 \rightarrow {}^7F_i$ ($i = 6, 5, 4, 3$) and especially the $^5D_4 \rightarrow {}^7 F_5$ (545 nm) one. This result suggests that this anneal treatment favors an optimum distribution of the ions in the matrix. Above this temperature, a quenching mechanism was observed until a complete disappearance (from 800 °C) of the Tb emission. Beyond 800 °C, we observed a structure deterioration of the ZnO host matrix due to a diffusion process between the Si substrate and the film as well as an increase of tensile stress of the film. We observed the emergence of radiative ZnO band gap (387 nm) transition. This transition increased significantly with annealing temperature until 1000 °C.

Furthermore, the maximum PL intensity of Tb ions occurred upon annealing at 600 °C. By contrast, the stress evolution analysis showed that a compressive stress was present in the film upon annealing treatment from room temperature up to 800 °C. At this latter temperature, a relaxation of the film was reached. Above this temperature, a tensile stress appeared. We conclude that there is no relationship between the stress state of the film and the Tb emission.

Currently, we are conducting several studies of the doping ratio effect on the PL properties. Time decay measurements will also be carried out for a deeper understanding of the transfer mechanisms in Tb:ZnO film.

Acknowledgments

References

[1] U. Ozgur, Y.I. Alivov, C. Liu, A. Teke, M.A. Reshchikov, S. Dogan, V. Avrutin, S.J. Cho, H. Morkoc, J. Appl. Phys. 98 (2005) 041301.
[2] D.K. Hawang, M.S. Oh, J.H. Lim, S.J. Park, J. Phys. D: Appl. Phys. 40 (2007) R 387.
[3] N.J. Awang, M. Aziz, A.R.M. Yusoff, Solid State Sci. Technol. 16 (2008) 45.
[4] J. Petersen, C. Brimont, M. Gallart, G. Schmerber, P. Gilliot, C. Ulhaq-Bouillet, J.L. Rehspringer, S. Colis, C. Becker, A. Slaoui, A. Dinia, J. Appl. Phys. 107 (2010) 123522.
[5] A.B. Djurisic, Y.H. Leung, Small 2 (2006) 944.
[6] Z.B. Fang, Y.S. Tang, H.X. Gong, C.M. Zhen, Z.W. He, Y.Y. Wang, Mater. Lett. 59 (2005) 2611.
[7] X.M. Teng, H.T. Fang, S.S. Pan, C. Ye, G.H. Li, J. Appl. Phys. 100 (2006) 053507.
[8] T. Minami, H. Sato, H. Nanto, S. Takata, Jpn. J. Appl. Phys. 24 (1985) L781.
[9] S.M. Liu, F.Q. Liu, Z.G. Wang, Chem. Phys. Lett. 343 (2001) 489.
[10] J. Zhang, H. Feng, W. Hao, T. Wang, Mater. Sci. Eng. A 425 (2006) 346.
[11] S. Zhao, L. Wang, L. Yong, Z. Wang, Physica B 405 (2010) 3200.
[12] A. Ortiz, C. Falcony, M. Garcia, A. Sanchez, J. Phys. D. Appl. Phys. 20 (1987) 670.
[13] A. Cetin, R. Kibar, S. Selvi, P.D. Townsend, N. Can, Physica B 404 (2009) 3379.
[14] J. Tauc, R. Grigorovici, A. Vancu, Phys. Status Solidi 15 (1966) 627.
[15] S.Y. Ting, P.J. Chen, H.C. Wang, C.H. Liao, W.M. Chang, Y.P. Hsieh, C.C. Yang, J. Nanomater. 2012 (2012) 6.
[16] F.H. Shan, G.X. Liu, B.C. Shin, W.J. Lee, J. Korean Phys. Soc. 54 (2009) 916.
[17] K.S. Kim, H.W. Kim, N.H. Kim, Physica B 334 (2003) 343.
[18] C. Besleaga, G.E. Stan, A.C. Galca, L. Ion, S. Antohe, Appl. Surf. Sci. 258 (2012) 8819.
[19] M. Ghosh, A.K. Raychaudhuri, J. Appl. Phys. 100 (2006) 034315.
[20] S. Li-Bin, L. Ming-Biao, R. Jun-Yuan, W. Li-Jin, X. Cui-Yan, Chin. Phys. B 18 (2009) 726.
[21] Y.F. Li, B. Yao, Y.M. Lu, Y.Q. Gai, C.X. Cong, Z.Z. Zhang, D.X. Zhao, J.Y. Zhang, B.H. Li, D.Z. Shen, X.W. Fan, Z.K. Tang, J. Appl. Phys. 104 (2008) 083516.
[22] Z.W. Liu, W.J. Fu, M. Liu, J.F. Gu, C.Y. Ma, Q.Y. Zhang, Surf. Coat. Technol. 202 (2008) 5410.
[23] R. Reisfeld, Z. Gur-Arieh, E. Greenberg, Anal. Chim. Acta. 50 (1970) 249.
[24] T. Hoshina, Jpn. J. Appl. Phys. 6 (1967).
[25] C.K. Duan, C.C. Ko, G. Jia, X. Chen, P.A. Tanner, Chem. Phys. Lett. 506 (2011) 179.

[26] S.M. Liu, F.Q. Liu, H.Q. Guo, Z.H. Zhang, A.G. Wang, Phys. Lett. A 271 (2000) 128.
[27] L. Yang, Y. Tang, A. Hu, X. Chen, K. Liang, L. Zhang, Physica B 403 (2008) 2230.
[28] Y.T. An, C. Labbé, M. Morales, P. Marie, F. Gourbilleau, Phys. Status Solidi C 9 (2012) 2207.
[29] A. Podhorodecki, N.V. Gaponenko, M. Banski, T. Kim, J. Misiewicz, ECS Trans. 28 (2010) 81.
[30] A. Podhorodecki, M. Banski, J. Misiewicz, J. Serafinczuk, N.V. Gaponenko, J. Electrochem. Soc. 157 (2010) H628.
[31] A.B. Djurisic, A.M.C. Ng, X.Y. Chen, Prog. Quantum Electron. 34 (2010) 191.
[32] H.X. Zhang, C.H. Kam, Y. Zhou, X.Q. Han, S. Buddhudu, Y.L. Lam, C.Y. Chan, Thin Solid Films 370 (2000) 50.
[33] H. Amekura, A. Eckau, R. Carius, Ch. Buchal, J. Appl. Phys. 84 (1998) 3867.